

# STATE OF THE CLIMATE IN 2013



Special Supplement to the  
*Bulletin of the American Meteorological Society*  
Vol. 95, No. 7, July 2014



traveled east towards the waters north of Samoa. TC Garry increased to a Category 2 strength system on 22 January with a minimum central pressure of 984 hPa and tropical storm force winds extending 50 nautical miles from the storm eye and sustained at 45 kt (23 m s<sup>-1</sup>) with wind gusts of up to 50 kt (26 m s<sup>-1</sup>). Garry peaked as a Severe Category 3 storm north of Suvarrow and Palmerston Island in the Northern Cook Islands, with average wind speeds estimated at 80 kt (41 m s<sup>-1</sup>) and gusts up to 110 kt (57 m s<sup>-1</sup>).

In January, a Category 1 TC, Oswald, made landfall on the Cape York Peninsula on 21 January with winds of 35 kt (18 m s<sup>-1</sup>). The storm traversed the peninsula and turned due south, traveling almost the entire length of Queensland over land as a deteriorating system. Significant impacts from waves and winds in Cairns included downed power lines and damage to coastal communities, with many extreme rainfall records broken that led to flooding and road closures. Total damages exceeded \$2.5 billion US dollars and six people died.

The final severe TC during the season formed on 7 March in the Queensland region and was named Sandra the next day as it rapidly intensified in the Coral Sea from a Category 1 to Category 2 tropical cyclone. Convection strengthened over TC Sandra's center as it was located northwest of Noumea, New Caledonia, while it moved eastward into RSMC Nadi's area of responsibility and further intensified into a Severe Category 3 system (minimum central pressure estimated at 968 hPa). Upon reaching Category 4 status on 9 March over the eastern Coral Sea, wave action and maximum sustained winds of 76 kt (39 m s<sup>-1</sup>) with gusts in excess of 108 kt (56 m s<sup>-1</sup>) impacted the Solomon Islands. Vanuatu received in excess of 380 mm of rainfall at some locations. The storm turned southeast, then due south, tracking along a trajectory to the west of New Caledonia when it peaked on 11 March with maximum sustained wind speeds of 105 kt (54 m s<sup>-1</sup>). On 13 March, TC Sandra then passed within 220 km of Lord Howe Island in the North Tasman Sea as a Category 1 storm on 14 March, bringing destructive wind gusts of 81 kt (42 m s<sup>-1</sup>) that downed trees and littered roads with debris along with heavy ocean swells that brought rough surf and rip currents to Australia's east coast. Remnants of the storm brought severe thunderstorms, tornadoes, and heavy rainfall to the Taranaki region of New Zealand's North Island.

e. *Tropical cyclone heat potential*—G. J. Goni, J. A. Knaff, and I-I Lin

This section summarizes the previously described TC basins from the standpoint of tropical cyclone heat potential (TCHP), by focusing on upper ocean temperature conditions during the season with respect to average values. The TCHP (Goni and Trinanes 2003), defined as the excess heat content above 26°C in the water column contained between the sea surface and the depth of the 26°C isotherm, has been linked to TC intensity changes (Shay et al. 2000; Goni and Trinanes 2003; and I-I Lin et al. 2008, 2009). In addition, the magnitude of the in situ TCHP has also been identified as impacting maximum potential intensity (MPI) through modulating the during-TC air-sea coupling flux supply (Mainelli et al. 2008; I-I Lin et al. 2013). In general, fields of TCHP show high spatial and temporal variability associated with oceanic mesoscale features, interannual variability, or long-term decadal variability that can be detected with satellite altimetry (Goni et al. 1996; I-I Lin et al. 2008; Goni et al. 2009; Pun et al. 2014).

To examine the TCHP interannual variability, anomalies (departures from the 1993–2012 mean values) are computed during the months of TC activity in each hemisphere: June–November in the Northern Hemisphere and November–April in the Southern Hemisphere. In general, these anomalies show large variability within and among the TC basins.

In most of the ocean basins, the number of tropical cyclones remained similar to last year, except for the tropical Atlantic. Most of the basins continue to exhibit positive TCHP anomalies, except for the Arabian Sea and large areas of the South Pacific Basin (Fig. 4.25). The North Atlantic Basin continued exhibiting positive anomaly values of TCHP as previous years. However, there was only one hurricane in the Gulf of Mexico and one in the tropical North Atlantic, compared with 12 hurricanes in this region during the 2012 season. The Gulf of Mexico (part of the North Atlantic Basin) continued exhibiting positive anomalies except for a region susceptible to the spatial variability of the Loop Current, which had negative anomalies. The WNP Basin usually exhibits anomalies related to ENSO variability, and has been undergoing a long-term decadal subsurface warming associated with the La Niña-like conditions over the last decade (Kosaka and Xie 2013; England et al. 2014). The TCHP over the west Pacific MDR (4°–19°N, 122°E–180°) has been observed to increase considerably as well (Pun et al. 2013; Goni et al. 2013). During 2013, this warming continued in the western North

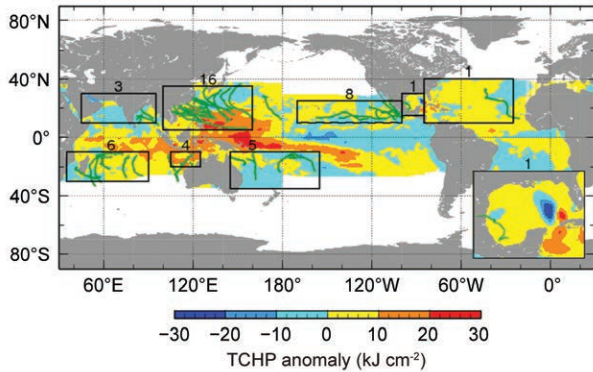


**FIG. 4.25. Global anomalies of TCHP corresponding to 2013** computed as described in the text. The boxes indicate the seven regions where TCs occur: from left to right, SIO, NIO, NWP, Southeast Indian, Southwest Pacific, ENP, and North Atlantic (shown as Gulf of Mexico and tropical Atlantic separately). The green lines indicate the trajectories of all tropical cyclones reaching at least Category 1 (1-minute average wind  $\geq 64$  kts) and above during Nov 2012–Apr 2013 in the Southern Hemisphere and Jun–Nov 2013 in the Northern Hemisphere. The numbers above each box correspond to the number of Category 1 and above cyclones that travel within each box. The Gulf of Mexico conditions during Jun–Nov 2013 are shown in the insert in the lower right corner.

Pacific and TCHP is currently at the highest level in 20 years. The TCHP fields in the west Pacific MDR since 1993, when altimetry became available, have increased by an average of 15%.

For each basin, the differences in the TCHP values between the most recent cyclone season and the previous season (Fig. 4.26) follow the same overall pattern as the differences between the 2012 and 2011 seasons (Goni et al. 2013). Some notable differences occurred in the NWP; west of Madagascar in the SIO; the NIO in the Bay of Bengal; and the northern tropical and subtropical areas of the North Atlantic, where TCHP values increased with respect to the previous season. The largest changes were in the South Pacific where warm anomalies are depicted in a large region toward the central equatorial Pacific while negative anomalies developed in the subtropics off the eastern coast of Australia.

During the 2013 season, the basins exhibited the following TCHP anomalies:

- As described in section 4d4, four TCs attained Category 5 super typhoon intensity. The most notable was Haiyan, which intensified over the WNP region from a Category 1 to a Category 5 storm associated with significant subsurface warming over a region of high TCHP values that ranged from 100–125  $\text{kJ cm}^{-2}$  (Fig. 4.27b).

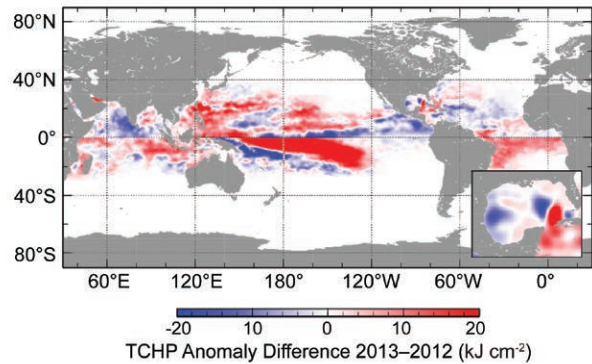


**FIG. 4.26. Differences between the TCHP fields in 2013 and 2012.**

In the WNP, as confirmed by two decades of the TAO/Triton mooring and satellite observations, the TCHP increased by about 10%, as compared to the early 90s (Pun et al. 2013). Haiyan’s fast translation speed ( $7\text{--}11 \text{ m s}^{-1}$ ) during intensification minimized the cooling effect. As Haiyan continued traveling over this favorable TCHP region with subsurface warmth for another 36 hours, its sustained winds reached the highest wind speed ever assigned to a TC by the JTWC with a value of 170 kt ( $85 \text{ m s}^{-1}$ ). Typhoon Usagi intensified over the same region, and within 24 hours, it also rapidly intensified into a Category 5 system. The pre-typhoon TCHP values ranged from 110–125  $\text{kJ cm}^{-2}$ , comparable to Haiyan (Fig. 4.27a).

- In the NIO Basin, TC Phailin (Fig. 4.27c) was the second strongest TC to make landfall in India on record. On 10 October, Phailin became a Category 1 tropical cyclone in the Bay of Bengal and one day later rapidly intensified to a Category 5 TC, with maximum sustained winds of 160 kt ( $82 \text{ m s}^{-1}$ ). This intensification coincided with its path traveling over warm waters with TCHP values slightly above 50  $\text{kJ cm}^{-2}$ . The intensification of this cyclone produced a cooling of the surface waters of approximately  $3^\circ\text{C}$ .
- In the SIO Basin, TC Felling formed in January 2013, reaching maximum intensity of 115 kt ( $59 \text{ m s}^{-1}$ ) at approximately  $16.2^\circ\text{S}$  on 30 January at 1200 UTC. The TCHP under this TC track only reached 50  $\text{kJ cm}^{-2}$  at the time of its maximum intensity (Fig. 4.27d); however, the storm developed a well-defined eye, with a deep, intense ring of convection forming in the eye-wall (<http://weather.noaa.gov/pub/data/raw/wt/wtio30.fmee.txt>). The associated cooling of  $3^\circ\text{C}$  and 25  $\text{kJ cm}^{-2}$  in SST and TCHP, respectively, are typical values for intense TCs.

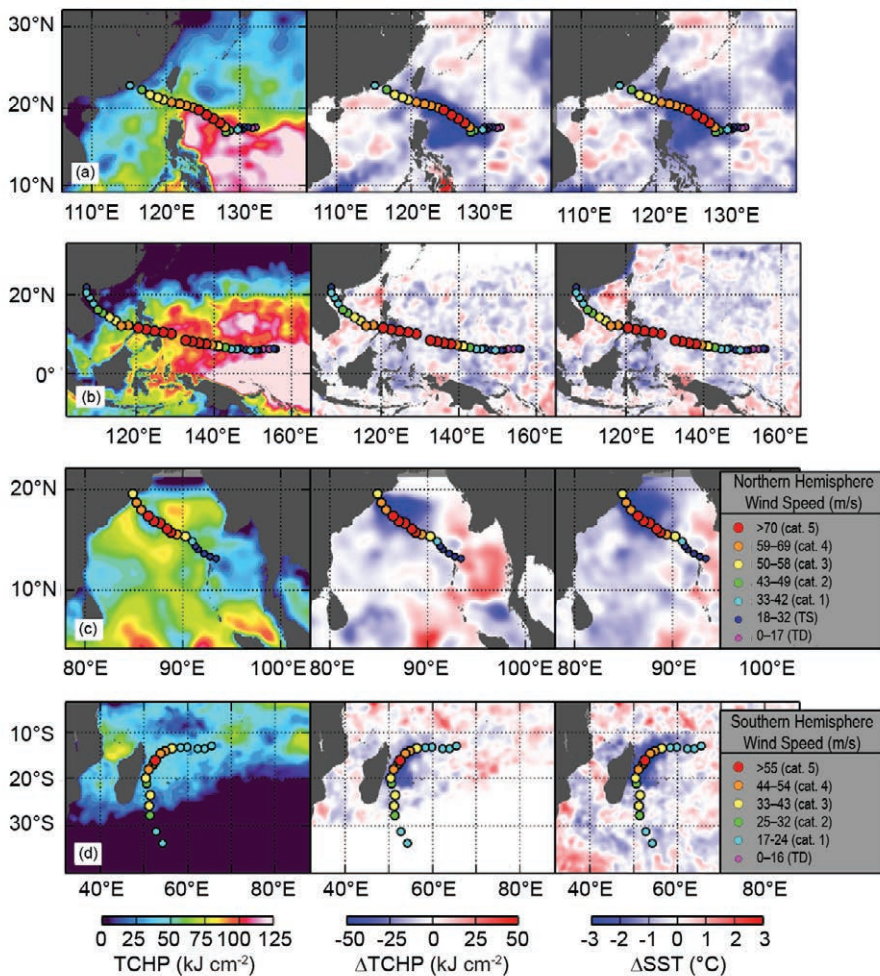


**FIG. 4.27.** (Left) TCHP and surface cooling given by the difference between post- and pre-storm values of (center) tropical cyclone heat potential and (right) sea surface temperature for tropical cyclones (a) Usagi, (b) Haiyan, (c) Phailin, and (d) Felleng. The TCHP values correspond to two days before each cyclone reaches its maximum intensity value.

*f. Global monsoon summary—B. Wang*

Global monsoon (GM) is the dominant mode of annual variation of the tropical-subtropical precipitation and circulation (Wang and Ding 2008), and thus a defining feature of seasonality and a major mode of variability of the Earth’s climate system. Figure 4.28 summarizes the monsoon rainfall anomalies for the period November 2012–October 2013, which is a global monsoon year that includes both the SH summer monsoon (SHSM) from November 2012 to April 2013 and the NH summer monsoon (NHSM) from May to October 2013.

The global land monsoon precipitation is strongly influenced by the status of ENSO, especially the land areas of Asia, Australia, northern Africa, and Central America (Wang et al. 2012). From November 2012 to October 2013, the equatorial Pacific SSTs were

near normal except for a moderate cooling in the far eastern Pacific. Given the ENSO-neutral status, no coordinated monsoon rainfall anomalies were expected on a global scale, and as such the global monsoon anomalies would be expected to be near average overall. This was indeed the case for 2013, as shown in Fig. 4.28. Significant monsoon rainfall anomalies, however, did occur on local and regional scales. The SHSM rainfall over land areas tended to be moderately below normal with deficient rainfall over northeast Australia and Madagascar. The NHSM rainfall over land shows a mixed pattern of regional anomalies: above-normal rainfall occurred over northern India and southwest Mexico while deficient rainfall occurred in the East Asian subtropics and Nigeria–Cameroon.

Figure 4.29 shows the time series of the monsoon precipitation and low-level circulation indices. Note that the precipitation indices represent the total amount of precipitation over both land and ocean. The definitions of circulation indices for each monsoon region are shown in Table 4.1 (Yim et al. 2013). In 2013, the majority of summer monsoon systems, including western North Pacific (WNP), North American (NA), northern African (NAF), southern African (SAF), and Australian (AUS), had normal seasonal mean strength with an average precipitation and circulation index value  $<0.5$  standard deviation. The precipitation and circulation indices together represent the strength of each regional monsoon system. The Indian (I) summer monsoon in 2013 was strong (the precipitation index was  $+0.8$  standard deviation and the circulation index was  $+2.5$  standard deviation). On the other hand, the East Asian (EA) summer monsoon and South American (SA) summer